

# Design of Polar Codes in 5G New Radio

Valerio Bioglio, *Member, IEEE*, Carlo Condo, *Member, IEEE*, Ingmar Land, *Senior Member, IEEE*

**Abstract**—Polar codes have attracted the attention of academia and industry alike in the past decade, such that the 5<sup>th</sup> generation wireless systems (5G) standardization process of the 3<sup>rd</sup> generation partnership project (3GPP) chose polar codes as a coding scheme. In this paper, we provide a user-friendly description of the encoding process foreseen by the 5G standard, to facilitate the simulation and implementation of 5G-compliant polar codes.

## I. INTRODUCTION

Polar codes are a class of capacity-achieving codes introduced in [1]. In the past decade, the interest and research effort on polar codes has been constantly rising in academia and industry alike. Within the ongoing 5<sup>th</sup> generation wireless systems (5G) standardization process of the 3<sup>rd</sup> generation partnership project (3GPP), polar codes have been adopted as channel coding for uplink and downlink control information for the enhanced mobile broadband (eMBB) communication service. 5G foresees two other frameworks, namely ultra-reliable low-latency communications (URLLC) and massive machine-type communications (mMTC), for which polar codes have been selected as one of the possible coding schemes.

The construction of a polar code involves the identification of channel reliability values associated to each bit to be encoded. This identification can be effectively performed given a code length and a specific signal-to-noise ratio. However, within the 5G framework, various code lengths, rates and channel conditions are foreseen, and having a different reliability vector for each parameter combination is unfeasible. Thus, substantial effort has been put in the design of polar codes that are easy to implement, having low description complexity, while maintaining good error-correction performance over multiple code and channel parameters.

The majority of available literature does not take in account the specific codes designed for 5G and their encoding process; given their upcoming widespread utilization, the research community would benefit from considering them within error-correction performance evaluations and encoder/decoder designs. Both the encoding and the decoding process can in fact incur substantial speed and complexity overhead, while the performance of decoders is tightly bound to the characteristics of the polar code. Hardware and software implementations works can effectively broaden their audience by including compliance to the 5G standard.

In this paper, we review the polar code encoding process foreseen by 5G, from the code concatenation, through interleaving functions, to the polar-code specific subchannel allocation and rate-matching schemes. The purpose of this work is to provide the reader with a straightforward, self-contained guide to the understanding and implementation

of 5G-compliant encoding of polar codes. We analyze the foreseen communication chain and give insights about its operating steps, along with decoding options. We assume that the reader has some familiarity with polar codes, and refer to [2] for an introduction.

The remainder of the paper is organized as follows. Section II introduces polar codes, along with concepts used in the 5G encoding process, such as interleaving and rate-matching. Section III details the a step-by-step guide to 5G polar code encoding. Conclusions are drawn in Section IV.

## II. PRELIMINARIES

In this Section, we introduce the basic concepts on polar codes. In particular, we review various approaches to frozen set design, decoding and rate matching. Moreover, considerations on the cyclic redundancy check code (CRC), distributed CRC and assistant bits used in the 5G are given as well, along with the description of 5G polar code use cases.

### A. Polar codes definition

Mathematical foundations of polar codes lay on the polarization effect [1] of the matrix  $\mathbf{G}_2 = \begin{bmatrix} 1 & 0 \\ 1 & 1 \end{bmatrix}$ . In an  $(N, K)$  polar code of length  $N = 2^n$ , the polarization effect establishes  $N$  virtual channels, through which a single bit  $u_i$  is transmitted. Each bit-channel, or subchannel, has a different reliability; message bits are allocated to the  $K$  most reliable channels. The polar code is hence defined by the transformation matrix  $\mathbf{G}_N = \mathbf{G}_2^{\otimes n}$ , i.e. as the  $n$ -th Kronecker power of the polarizing matrix, and either the frozen set  $\mathcal{F}$  of size  $N - K$ , or its complementary information set  $\mathcal{I} = \mathcal{F}^C$  of size  $K$ , where  $\mathcal{I}$  and  $\mathcal{F}$  are subsets of the index set  $\{0, 1, \dots, 2^{n-1}\}$ . A codeword  $\mathbf{d} = \{d_0, d_1, \dots, d_{N-1}\}$  is calculated as

$$\mathbf{d} = \mathbf{u}\mathbf{G}_N, \quad (1)$$

where the input vector  $\mathbf{u} = \{u_0, u_1, \dots, u_{N-1}\}$  is generated by assigning  $u_i = 0$  if  $i \in \mathcal{F}$ , and storing information in the remaining elements. Each index  $i$  identifies a different bit-channel.

### B. Frozen set design

As  $N$  goes toward infinity, the polarization phenomenon influences the reliability of bit-channels, that are either completely noisy or completely noiseless; even more, the fraction of noiseless bit-channels equals the channel capacity [1]. More formally, let  $W$  be a binary memoryless symmetric channel with input alphabet  $\mathcal{X} = \{0, 1\}$  and output alphabet  $\mathcal{Y}$ , and let  $\{W(y | x) : x \in \mathcal{X}, y \in \mathcal{Y}\}$  be the transition probabilities. In order to quantify the reliability, i.e. the goodness, of the

channel  $W$ , we use the Bhattacharyya parameter  $Z(W) \in [0, 1]$ , that is defined as

$$Z(W) = \sum_{y \in \mathcal{Y}} \sqrt{W(y \mid 0)W(y \mid 1)}. \quad (2)$$

Hence, the good bit-channels are the ones that have the lowest Bhattacharyya parameter.

For finite practical code lengths, the polarization of bit-channels is incomplete, therefore, there are bit-channels that are partially noisy. The polar encoding process consists in the classification of the bit-channels in  $\mathbf{u}$  into two groups: the  $K$  good bit-channels that will carry the information bits and are indexed by the information set  $\mathcal{I}$ , and the  $N - K$  bad bit-channels that are fixed to a predefined value (usually 0) and are indexed by the frozen set  $\mathcal{F}$ . In case of finite code lengths, the  $K$  best bit-channels, i.e. the ones with the highest reliability, are selected to form the information set, while the remaining bit-channels are frozen.

Non-universality of polar codes, i.e. the fact that bit-channels non-linearly depend on the initial channel condition, poses huge problems in the construction of practical polar codes. As a consequence, many methods to design the frozen sets on-the-fly with limited complexity have been proposed [3]. Along with the Bhattacharyya parameter, Arikan initially proposed to use Monte-Carlo simulations to estimate bit-channel reliabilities [1]. The density evolution (DE) method, initially proposed in [4] and improved in [5], can provide theoretical guarantees on the estimation accuracy, however at a high computational cost. A bit-channel reliability estimation method for AWGN channels based on Gaussian approximation (GA) of DE has been proposed in [6], giving accurate results with limited complexity. However, even this method is still too complex to be run on-the-fly on the basis of the channel conditions.

Recent attempts to study the partial order imposed by the polarization effect in order to design universal polar codes have been useful for practical application of polar codes [7]–[9]. Moreover, taking in account distance properties in short polar codes design may give superior error-correction performance [10], [11]. Finally, bit-channel analysis usually does not take into account the use of list decoders or assistant bits in the decoding [12]. As we will see, these studies and intensive simulations lead the 5G standardization to propose a universal bit channel reliability sequence.

### C. Decoding

The first proposed decoding algorithm for polar codes is the successive cancellation algorithm (SC) [1], with which polar codes achieve channel capacity at infinite code length. It can be represented as a binary tree search, where the leaf nodes are the  $N$  bits to be estimated, and soft information about the received vector is input at the root node. Fig. 1 shows the SC decoding tree for an  $(8, 4)$  polar code. We consider the soft values received from the channel and the internally exchanged information to be logarithmic likelihood ratios (LLRs). At each stage  $t$ , the LLR values  $\alpha = \{\alpha_0, \alpha_1, \dots, \alpha_{2^t-1}\}$  are sent from parent to child nodes, while the hard decision values

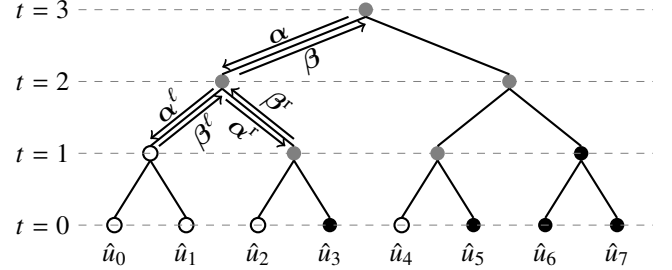


Fig. 1: SC decoder of an  $(8, 4)$  polar code,  $\mathcal{F} = \{u_0, u_1, u_2, u_4\}$ .

$\beta = \{\beta_0, \beta_1, \dots, \beta_{2^t-1}\}$  go from child nodes to the parent node.

The  $2^{t-1}$ -element LLR vector going to the left child node  $\alpha^l = \{\alpha_0^l, \alpha_1^l, \dots, \alpha_{2^{t-1}-1}^l\}$ , and the one going to the right child node  $\alpha^r = \{\alpha_0^r, \alpha_1^r, \dots, \alpha_{2^{t-1}-1}^r\}$ , are computed as

$$\alpha_i^l = 2 \operatorname{arctanh} \left( \tanh \left( \frac{\alpha_i}{2} \right) \tanh \left( \frac{\alpha_{i+2^{t-1}}}{2} \right) \right), \quad (3)$$

$$\approx \operatorname{sgn}(\alpha_i) \operatorname{sgn}(\alpha_{i+2^{t-1}}) \min(|\alpha_i|, |\alpha_{i+2^{t-1}}|), \quad (4)$$

$$\alpha_i^r = \alpha_{i+2^{t-1}} + (1 - 2\beta_i) \alpha_i. \quad (5)$$

The  $2^t$  elements of  $\beta$  are instead computed through  $\beta^l = \{\beta_0^l, \beta_1^l, \dots, \beta_{2^{t-1}-1}^l\}$  and  $\beta^r = \{\beta_0^r, \beta_1^r, \dots, \beta_{2^{t-1}-1}^r\}$  as

$$\beta_i = \begin{cases} \beta_i^l \oplus \beta_i^r, & \text{if } i < 2^{t-1}, \\ \beta_{i-2^{t-1}}^r, & \text{otherwise,} \end{cases} \quad (6)$$

where  $\oplus$  represents the bitwise exclusive OR (XOR) operation. The estimation of the  $i$ -th bit  $\hat{u}_i$  at leaf nodes is performed as

$$\hat{u}_i = \begin{cases} 0, & \text{if } i \in \mathcal{F} \text{ or } \alpha_i \geq 0, \\ 1, & \text{otherwise.} \end{cases} \quad (7)$$

The SC algorithm can be implemented in both software and hardware with low complexity [13], [14], but its error-correction performance is mediocre when decoding practical code lengths. Thus, many attempts have been made to overcome this shortcoming [15], [16].

Eventually, a list-based decoding approach to polar codes (SCL) was introduced in [17]. A set of SC decoders works in parallel maintaining different codeword candidates at the same time. Every time a leaf node is reached, the bit is estimated as both 1 and 0, doubling the number of codeword candidates. A path metric for each candidate is updated, based on the value of the LLR associated to the node. The less likely candidates are then discarded to limit the growth in complexity of the algorithm. SCL substantially improves the error-correction performance of SC at moderate code lengths, especially when the code is concatenated to a CRC. This algorithm has been taken as a baseline in 5G error-correction performance evaluations, in particular with a list size equal to 8. While the effectiveness of SCL improves as the list size increases, its implementation complexity increases as well. To limit the rise in complexity, various approaches have been proposed for software and hardware decoders alike. Partitioned SCL [18] and its evolutions [19], [20] consider different list sizes at different stages of the SC tree, reducing the memory

requirements at higher stages. SC-Stack decoding [21] expands only the most probable candidate thanks to a priority queue. Adaptive SCL decoding [22] foresees increasing list sizes in case of failed decoding, while a hardware decoder with flexible list size has been proposed in [23].

SC-based decoding algorithms suffer from long latency, due to their serial nature. Fast decoding algorithms for SC, SC-Flip and SCL have been proposed in [24]–[30]. They rely on the identification of special nodes, i.e. patterns of frozen and information bits, and the efficient decoding of these nodes. These techniques prune the SC decoding tree, and substantially decrease latency, at the expense of more complex hardware implementations. Multi-bit decoding [31], [32] traverses the whole tree, but allows to estimate a higher number of bits in parallel, effectively reducing the number of stages of the tree.

Belief propagation (BP) decoding of polar codes has been proposed as well [1]. The algorithm iterates on the polar code Tanner graph, exchanging soft information in both directions. BP decoding of polar codes can potentially achieve faster decoding than SC-based algorithms, since it is inherently possible to parallelize operations, at the cost of a higher implementation complexity [33]. However, polar codes constructed for SC suffer severe error-correction performance degradation when decoded with BP, and construction of polar codes for BP is difficult, due to the complexity of the factor graph [34]. In limited cases, the degradation can be recovered, at the cost of an augmented number of iterations, leading to poor throughput [35].

#### D. Rate matching

According to their definition, the length  $N$  of a polar code is limited to powers of two, while the code dimension  $K$  can assume any value smaller than  $N$ , since only the  $K$  most reliable bits will be used to carry the information. This is a limitation for typical 5G applications, where the amount of information  $K$  is fixed and a codeword of length  $N$  is needed to achieve the desired rate  $R = K/N$ . Rate matching for polar codes becomes thus a length matching problem, and can be faced through classical coding theory techniques as puncturing and shortening [36].

Both puncturing and shortening reduce the length of a mother code by not transmitting code bits in a predetermined pattern, called matching pattern; the difference lies in the meaning of the code bits belonging to the matching pattern. In puncturing, one or more code bits are not transmitted, which are treated as erased at the decoder. In shortening, a sub-code is introduced such that one or more code bits assume a fixed value, typically zero, and not transmitted since they are known at the decoder. Rate matching alters the reliability of the subchannels, with an impact that depends on the strategy adopted. As a rule of thumb, it has been observed that for polar codes, shortening works better for high rates, puncturing for low rates [37].

Puncturing deteriorates subchannel reliabilities; moreover, the erasures introduced by puncturing cause some bit channels, called incapable bits, to be completely unreliable. It can be shown that  $U$  punctured code bits make exactly  $U$  subchannels

incapable; the position of these bits can be calculated on the basis of the matching pattern [38]. In order to avoid catastrophic error-correction performance degradation under SC decoding, incapable bits must be frozen in order to avoid random decisions at the decoder.

Shortening improves the bit channel reliabilities by introducing overcapable bits, i.e. bits with (theoretically) infinite reliability: those bits are surely correctly decoded under SC, if the previous bits have been correctly decoded [37]. However, code bits in the matching pattern must depend on frozen bits only, which forces to freeze the usually most reliable subchannels.

Three main strategies have been proposed to design the matching pattern. The first option is to design the frozen set of the mother polar code based on the matching pattern. According to this strategy, the matching pattern is initially generated according to a some heuristic, then the subchannel reliabilities are calculated in order to find the optimal frozen set. This method has been proposed in [39] for shortening and in [38], [40] for puncturing of polar codes, where the DE/GA algorithm is run to find the optimal frozen set on the basis of different matching patterns. The result is a code with good block error rate (BLER) performance, at the cost of an higher complexity due to the reliability calculation. An alternative approach, proposed in [41], [42], is to design the matching pattern on the basis of the frozen set. This significantly reduces the code design complexity, albeit at the cost of an increased BLER. As we will see, this is the approach selected by 3GPP for the standardization of polar codes in 5G. Finally, joint optimization, presented in [43], proposes to design frozen set and matching pattern at the same time. Symmetries in the polar code structure reduce the number of matching patterns to be tested, however not enough to make this technique practical for application in 5G.

#### E. Assistant bits design

It has been noticed that the introduction of an outer CRC code improves the error-correction performance [44], for example when used to help the selection of the correct candidate in SCL decoding. In general, it has been proven that the minimum distance of polar codes can be dramatically improved by adding an outer code to polar codes [45]. This improved code spectrum is fully used by SCL decoders [17], and it has contributed to the selection of polar codes for 5G.

Assistant bits can be broadly identified as additional bits that help the decoding of the polar code, either increasing the error-correction performance or improving a metric, like speed or complexity. The introduction of an outer code can be seen as the addition of assistant bits to information bits. After the initial proposal of CRC as assistant bits made in [17], many other outer codes have been proposed [46]. Parity-checks (PC) have emerged as an alternative to design assistant bits due to their simplicity and flexibility [45], [47]. Introducing parity check bits in the middle of the decoding instead of a unique CRC check at the end makes it easier to tune the polar code spectrum. It has been shown that subchannels corresponding to minimum weight rows are the best candidates

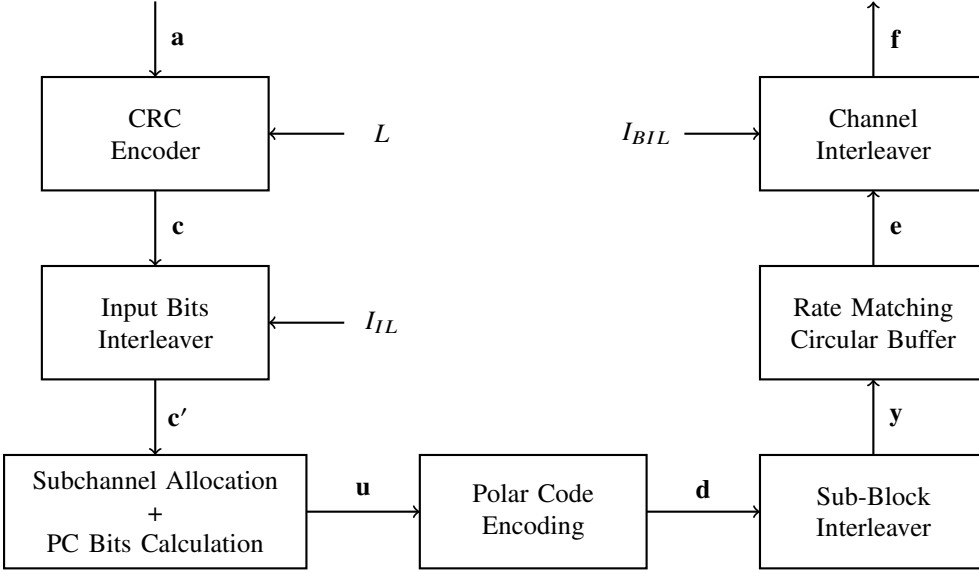


Fig. 2: Polar code encoding process in 5G.

to host parity checks [48]. In [49], a low complexity parity check design based on shift registers is proposed, showing that good performance can be obtained adding really simple parity checks to the information set. A further step is to mix CRC and parity checks, as proposed in [50], to improve the flexibility of the polar code design.

The insertion of an interleaver between the CRC encoder and the polar encoder may have a positive impact on the performance of the code due to the change of the number of minimum weight codewords induced by the interleaver [51]. The interleaver is used to turn the CRC into a distributed CRC, in that a CRC remainder bit is assigned to a bit-channel as soon as all the information bits involved in its parity check have been assigned as well. This feature can be used to reduce the decoding complexity by early terminating the decoding if an incorrect check is met, providing an additional false alarm rate (FAR) mitigation [52]. Furthermore, the distributed CRC bits scheme can be used to prune the SCL decoding tree [45].

#### F. Polar coded modulation

If low-order modulation schemes like 4QAM are used, the BLER is not affected by the modulation scheme since all bits in modulated symbols have uniform reliability. Polar-coded modulation (PCM) was introduced in [53] for larger constellations, exploiting the polarization effect in the construction of polar codes for higher-order modulation [54]. However, the canonical PCM requires the introduction of an additional polarization matrix whose size depends on the modulation scheme used [55]. This results in increased latency due to a further decoding step [56].

The introduction of a channel interleaver emerged as a low-complexity alternative to PCM; this technique, termed as bit-interleaved polar-coded modulation (BIPCM) [57], proved to improve the diversity gain under high-order modulation without increasing the code complexity [58]. In BIPCM, the channel is considered as a set of parallel bit channels which

can be combined with polar coded bits. Carefully mapping coded bits to modulation symbols offers a certain gain over the conventional random interleaving for high-order QAM over AWGN channels [59]. Moreover, interleavers designed to be adaptive to channel selectivity can achieve a remarkable diversity gain compared to random interleaving for polar-coded OFDM transmission [60]. The correlation between coded bits mapped into the same symbol allows to combine the demapping and deinterleaving units with the SC decoder to perform the decoding directly on the LLRs of the received symbols instead of the ones of the coded bits [61].

### III. POLAR CODE ENCODING IN 5G

Figure 2 portrays the set of operations that information encoded with polar codes goes through within the 5G framework. In the following, the notation introduced in the 3GPP technical specification [62] will be used. Polar codes in the uplink are used to encode the uplink control information (UCI) over the physical uplink control channel (PUCCH) and the physical uplink shared channel (PUSCH). In the downlink, polar codes are used to encode the downlink control information (DCI) over the physical downlink control channel (PDCCH), and the payload in the physical broadcast channel (PBCH). Table I summarizes the encoding chain parameters depending on channel and code parameters.

In more detail,  $A$  bits have to be transmitted through a code of length  $E$  code bits.  $L$  CRC bits are added to the information bits, resulting in  $K$  bits that will be encoded by a  $(N, K)$  mother polar code, with  $N = 2^n$ . Rate matching is finally performed to obtain a code of length  $E$  and rate  $R = A/E$ . Vector  $\mathbf{a}$  contains the  $A$  information bits to be transmitted. To every  $A$ -bit vector, an  $L$ -bit CRC is attached. The resulting vector  $\mathbf{c}$ , constituted of  $K = A + L$  bits, is passed through an interleaver. On the basis of the desired code rate  $R$  and codeword length  $E$ , a mother polar code of length  $N$  is designed, along with the relative bit channel reliability sequence and frozen set.

TABLE I: Channel parameters.

PUCCH/PUSCH		PDCCH/PBCH	
A $\geq 20$	12 $\leq A \leq 19$		PDCCCH/PBCH
	E - A $\leq 175$	E - A $> 175$	
$n_{max}$	10		9
$I_{IL}$	0		1
$I_{BIL}$	1		0
$L$	11	6	24
$n_{PC}$	0	3	0
$n_{PC}^{wm}$	0	0	1

The interleaved vector  $\mathbf{c}'$  is assigned to the information set along with ad-hoc parity-check bits, while the remaining bits in the  $N$ -bit  $\mathbf{u}$  vector are frozen. Vector  $\mathbf{u}$  is encoded with  $\mathbf{d} = \mathbf{u}\mathbf{G}_N$ , where  $\mathbf{G}_N = \mathbf{G}_2^{\otimes n}$  is the generator matrix for the selected mother code. After encoding, a sub-block interleaver divides  $\mathbf{d}$  in 32 equal-length blocks, scrambling them and creating  $\mathbf{y}$ , that is fed into the circular buffer. For rate matching, puncturing, shortening or repetition are applied to change the  $N$ -bit vector  $\mathbf{y}$  into the  $E$ -bit vector  $\mathbf{e}$ . A channel interleaver is finally applied to compute the vector  $\mathbf{f}$ , that is now ready to be modulated and transmitted.

In the following, we detail the operations necessary in each step of the 5G encoding chain.

#### A. Code parameters and rate matching selection

The 5G polar code encoding process relies on several parameters that depend on the amount and type of information to be transmitted and on the used channel. The first parameter that needs to be identified is the code length of the mother polar code,  $N = 2^n$ . The number  $n$  is calculated as

$$n = \max(\min(n_1, n_2, n_{max}), n_{min}), \quad (8)$$

where  $n_{min}$  and  $n_{max}$  give a lower and an upper bound on the mother code length, respectively. In particular,  $n_{min} = 5$ , while  $n_{max} = 9$  for the downlink control channel, and  $n_{max} = 10$  for the uplink. Parameter  $n_2$  gives an upper bound on the code based on the minimum code rate admitted by the encoder, i.e.  $\frac{1}{8}$ ; as a consequence,  $n_2 = \lceil \log_2(8K) \rceil$ . Finally, the value of  $n_1$  is bound to the selection of the rate-matching scheme. It is in fact usually calculated as  $n_1 = \lceil \log_2(E) \rceil$ , so that  $2^{n_1}$  is the smallest power of two larger than  $E$ . However, a correction factor is introduced to avoid a too severe rate matching: if  $\{\log_2(E)\} < 0.17$ , i.e. if the smallest power of two larger than  $E$  is too far from  $E$ , the parameter is set to  $n_1 = \lfloor \log_2(E) \rfloor$ . In this case an additional constraint on the code dimension is added, imposing  $K < \frac{9}{16}E$ , to assure that  $K < N$ .

If a code length  $N > E$  is selected, the mother polar code will be punctured or shortened, depending on the code rate, before the transmission. In particular, if  $\frac{K}{E} \leq \frac{7}{16}$ , the code will be punctured, otherwise it will be shortened. On the contrary, if  $N < E$ , repetition is applied and some encoded bits will be transmitted twice; in this case, the code construction assures that  $K < N$ .

$\{x\} = x - \lfloor x \rfloor$  represents the fractional part of a real number  $x$ .

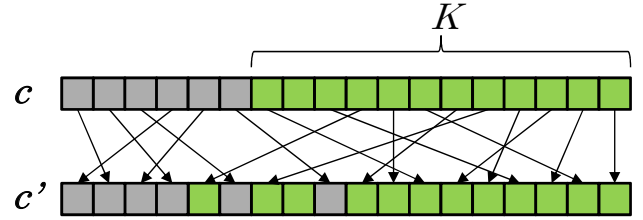


Fig. 3: Input bits interleaver design.

As shown in Table I, a set of flags and parameters assume different values depending on the type of transmission. The flags  $I_{IL}$  and  $I_{BIL}$  refer to the activation of the input bits interleaver and the channel interleaver respectively. The number of the two types of assistant PC bits are given by  $n_{PC}$  and  $n_{PC}^{wm}$  (see Section III-D for details).

The length of the information vector  $A$  and the length of the transmitted codeword  $E$  are dependent on the type, content, and number of consecutive transmissions, and are thus bound to decisions taken in layers higher than the physical one. The reader can consult [63] for detailed information. This guide enables 5G-compliant encoding for any allowed combination of  $A$ ,  $R$  and  $E$ .

#### B. CRC encoding

A CRC of  $L$  bits is appended to the  $A$  message bits stored in  $\mathbf{a}$ , resulting in a vector  $\mathbf{c}$  of  $A + L$  bits. The possible CRC generator polynomials are the following:

$$\begin{aligned} g_6(x) &= x^6 + x^4 + 1 \\ g_{11}(x) &= x^{11} + x^{10} + x^9 + x^5 + 1 \\ g_{24}(x) &= x^{24} + x^{23} + x^{21} + x^{20} + x^{17} + x^{15} + x^{13} + x^{12} + x^8 + \\ &\quad + x^4 + x^2 + x + 1 \end{aligned}$$

The polynomial  $g_{24}(x)$  is used for the payload in PBCH and DCIs in the PDCCH, while polynomials  $g_6(x)$  and  $g_{11}(x)$  are used for UCIs, in the case  $12 \leq A \leq 19$  and  $A \geq 20$ , respectively. The CRC shift register is initialized by all zeros for UCIs and for the PBCH payloads, and to all ones for the DCIs. Moreover, for DCIs, the CRC parity bits are “scrambled” according to a radio network temporary identifier (RNTI)  $x_0^{rnti}, x_1^{rnti}, \dots, x_{15}^{rnti}$ , i.e. the RNTI is masked in the last 16 CRC bits calculated by  $g_{24}(x)$  as  $c_{A+8+k} = c_{A+8+k} \oplus x_k^{rnti}$  for  $k = 0, \dots, 15$ .

#### C. Input bits Interleaver

The  $K$  bits obtained from the CRC encoder are interleaved before being inserted into the information set of the mother polar code. The interleaver is activated through a flag  $I_{IL}$ . In particular, the input bit interleaver is activated for PBCH payloads and PDCCH DCIs ( $I_{IL} = 1$ ), while it is bypassed in the case of PUCCH and PUSCH UCIs ( $I_{IL} = 0$ ).

The input bit interleaver interleaves up to  $K_{IL}^{max}$  input bits, where the interleaving pattern  $\Pi$  is calculated on the basis of the sequence  $\Pi_{IL}^{max}$  presented in Table II. The maximum number of input bits  $K$  is set to  $K_{IL}^{max} = 164$ , i.e.  $K \leq 164$ . In more detail, the parameter  $h = K_{IL}^{max} - K$  is calculated.

TABLE II: Input bits interleaver pattern mother sequence (bold integers represent CRC bit indeces).

$\Pi_{IL}^{max}$												
0	2	4	7	9	14	19	20	24	25	26	28	
31	34	42	45	49	50	51	53	54	56	58	59	
61	62	65	66	67	69	70	71	72	76	77	81	
82	83	87	88	89	91	93	95	98	101	104	106	
108	110	111	113	115	118	119	120	122	123	126	127	
129	132	134	138	139	<b>140</b>	1	3	5	8	10	15	
21	27	29	32	35	43	46	52	55	57	60	63	
68	73	78	84	90	92	94	96	99	102	105	107	
109	112	114	116	121	124	128	130	133	135	<b>141</b>	6	
11	16	22	30	33	36	44	47	64	74	79	85	
97	100	103	117	125	131	136	<b>142</b>	12	13	18	23	
38	39	80	137	<b>145</b>	17	40	75	<b>146</b>	48	<b>149</b>	37	
86	<b>143</b>	<b>144</b>	41	<b>147</b>	<b>148</b>	<b>150</b>	<b>151</b>	<b>152</b>	<b>153</b>	<b>154</b>	<b>155</b>	
<b>156</b>	<b>157</b>	<b>158</b>	<b>159</b>	<b>160</b>	<b>161</b>	<b>162</b>	<b>163</b>					

Starting from the entry at index 0, all elements of  $\Pi_{IL}^{max}$  are compared to  $h$ , and in the case that they are larger, they are stored in  $\Pi$ . Finally,  $h$  is subtracted from all the entries of  $\Pi$ , such that  $\Pi$  contains all the integers smaller than  $K$  in permuted order. The construction of the interleaving pattern  $\Pi$  is illustrated in Figure 3. This scrambling sequence has been proposed to facilitate early termination, both during normal decoding and on broadcast and DCI blind detection. This is made possible by the fact that after interleaving, every CRC remainder bit is placed after its relevant information bits. The interleaving function is applied to  $\mathbf{c}$ , and the  $K$ -bit vector  $\mathbf{c}' = \{c_{\Pi(0)}, \dots, c_{\Pi(K-1)}\}$  is obtained.

#### D. Subchannel allocation and PC bits calculation

In this procedure, vector  $\mathbf{c}'$  is expanded in the  $N$ -bit input vector  $\mathbf{u}$  with the addition of assistant bits and frozen bits. As a first step,  $n_{PC}$  parity-check bits are inserted within the  $K$  information and CRC bits. The mother polar code is hence a  $(N, K')$  code, with  $K' = K + n_{PC}$ .

To create the input vector  $\mathbf{u}$  to be encoded, the frozen set of subchannels needs to be identified. The number and position of frozen bits depend on  $N$ ,  $E$ , and the selected rate-matching scheme. Initially, the frozen set  $\bar{Q}_F^N$  and the complementary information set  $\bar{Q}_F^N$  are computed based on the polar reliability sequence  $Q_0^{N_{max}-1}$  [64] and the rate matching strategy. Later, information bits are assigned to  $\mathbf{u}$  according to the information set. Finally, assistant parity check bits are calculated and stored in  $\mathbf{u}$ , if necessary. In the following, we examine every step of the creation of the input vector  $\mathbf{u}$  in more detail.

1) *Frozen set  $\bar{Q}_F^N$* : The first bits identified in the frozen set correspond to the indices of the  $U = N - E$  untransmitted bits, i.e. the bits eliminated from the codeword by the rate-matching scheme. These indices correspond to the first  $U$  or the last  $U$  codeword bits in the case of puncturing and shortening, respectively, as explained in Section III-G. Due to the presence of an interleaver  $P$  between the encoding and the rate matching, the actual indices to be added to the frozen set correspond to the first or the last after interleaving; details on this sub-block interleaver can be found in Section III-F. If  $\frac{K}{E} \leq \frac{7}{16}$  and hence the mother polar code has to be punctured,

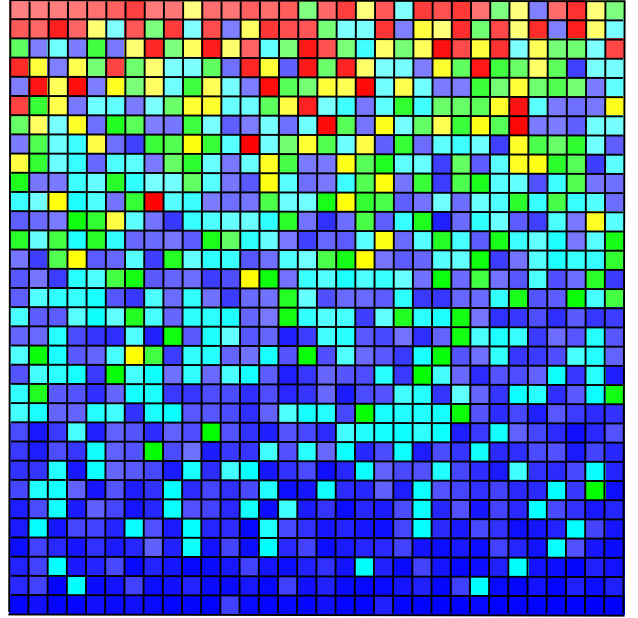


Fig. 4: Polar reliability sequence  $Q_0^{N_{max}-1}$ . Red, yellow, green, cyan and blue squares represent entries smaller than 64, 128, 256, 512 and 1024 respectively. Color brightness/intensity reveals integer largeness in the color interval.

additional indices are included in the frozen set such that  $\{0, \dots, T\} \subset \bar{Q}_F^N$ , with

$$T = \begin{cases} \left\lfloor \frac{3}{4}N - \frac{E}{2} \right\rfloor & \text{if } E \geq \frac{3}{4}N \\ \left\lfloor \frac{9}{16}N - \frac{E}{4} \right\rfloor & \text{otherwise} \end{cases} \quad (9)$$

This extra freezing is necessary to prevent bits in the information set to become incapable due to puncturing. Finally, new indices are added to the frozen set from the reliability sequence, starting from the least reliable, until  $|\bar{Q}_F^N| = N - K'$ .

The polar reliability sequence  $Q_0^{N_{max}-1}$  is a list of integers smaller than 1024 sorted in reliability order, from the least reliable to the most reliable; indices larger than  $N$  are skipped in the creation of  $\bar{Q}_F^N$ . A qualitative depiction of the reliability sequence and the subchannel selection process is illustrated in Figure 4. The 1024 squares represent all the subchannels of the mother code, from the least reliable in the top-left corner, to the most reliable in the bottom-right corner. There are 64 red subchannels, that are relative to the bit indices 0 to 63. The 64 yellow ones are relative to bit indices 64 to 127, the 128 green ones to bits 128 to 255, the 256 azure ones to bits 256 to 511, and the 512 blue ones to bits 512 to 1023. Darker shades of each color represent larger indices, while lighter shades are smaller ones. In the case that  $N = 512$  is selected, the 512 blue subchannels are excluded, while the red, yellow, green and azure ones are extracted maintaining their relative order, for a total of 512 ordered indices. In the case that  $N = 256$  is selected, only the red, yellow and green ones are extracted, and so on.

To summarize, the frozen set  $\bar{Q}_F^N$  is designed in three steps:

- 1) Pre-freezing:  $Q_1 = \{P(\gamma), \dots, P(\gamma+U-1)\}$  where  $\gamma = 0$  if  $\frac{K}{E} > \frac{7}{16}$  and  $\gamma = E$  otherwise.

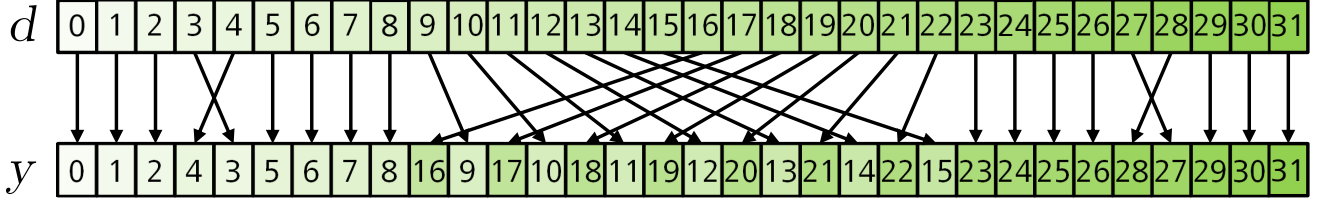


Fig. 5: Design of the sub-block interleaver.

- 2) Extra freezing:  $Q_2 = \{0, \dots, T\}$  where  $T$  is calculated according to (9) if  $\frac{K}{E} \leq \frac{7}{16}$ , otherwise  $Q_2 = \emptyset$ .
- 3) Reliability freezing:  $Q_3$  contains the first  $N - K' - |Q_1 \cup Q_2|$  elements of  $Q_0^{N_{max}-1}$  smaller than  $N$  not already included in  $Q_1 \cup Q_2$ .

Finally, the frozen set is given by  $\bar{Q}_F^N = Q_1 \cup Q_2 \cup Q_3$ . The bits of  $\mathbf{u}$  corresponding to these indices are set to zero, i.e.  $u_i = 0$  for all  $i \in \bar{Q}_F^N$ .

2) *Subchannel allocation*: The information set  $\bar{Q}_I^N$  is calculated as the complement of  $\bar{Q}_F^N$ , and contains  $K' = K + n_{PC}$  elements, corresponding to the bit indices that will contain the message bits and the parity check (PC) bits. The subchannels to be assigned to PC bits are calculated according to two different strategies:  $n_{PC}^{wm}$  are bound to the weight of rows of the generator matrix, while  $n_{PC}^{lr} = n_{PC} - n_{PC}^{wm}$  are bound to the subchannel reliability. The set of the parity check indices is called  $Q_{PC}^N$ , with  $Q_{PC}^N \subset \bar{Q}_I^N$ . To begin with,  $n_{PC}^{lr}$  bit indices are initially selected as the  $n_{PC}^{lr}$  least reliable subchannels in  $\bar{Q}_I^N$ . The index of the remaining  $n_{PC}^{wm}$  PC bit is selected as the subchannels corresponding to the row of minimum weight in the transformation matrix among the  $K$  most reliable bit indices in  $\bar{Q}_I^N$ . In the case of uncertainty due to the presence of too many rows with the same weight, the index with the highest reliability is selected. The row weight  $w(g_i)$  of subchannel  $i$  corresponds to the number of ones of the  $i$ -th row  $g_i$  of the transformation matrix  $\mathbf{G}_N$ , and it can be easily calculated as  $w(g_i) = 2^{o_i}$ , where  $o_i$  denotes the number of ones in the binary expansion of  $i$  [65].

After the subchannels have been allocated, the  $K$  message bits are stored in vector  $\mathbf{u}$ , i.e. the message is stored in the  $K$  indices of  $\bar{Q}_I^N \setminus Q_{PC}^N$ . To calculate the parity check bits, and thus assign a value to the remaining  $n_{PC}$  indices of  $\mathbf{u}$ , the methodology explained in Section III-D3 needs to be followed.

3) *PC bit calculation*: The calculation of the PC bits is performed through a cyclic shift register of length 5, initialized to 0. Each PC bit is calculated as the XOR of the message bits assigned to preceding subchannels, modulo 5, excluding the previously calculated parity check bits. To summarize, a PC bit  $u_i$ , with  $i \in Q_{PC}^N$ , is calculated as

$$u_i = \bigoplus_{j=\lfloor i_{PC}/5 \rfloor}^{q-1} u_{5j+p}, \quad (10)$$

where  $q = \lfloor i/5 \rfloor$ ,  $p = i \bmod 5$  and  $i_{PC} \in Q_{PC}^N$  is the highest index smaller than  $i$  for which  $i_{PC} \bmod 5 = p$ . If no such index exists,  $i_{PC} = 0$ .

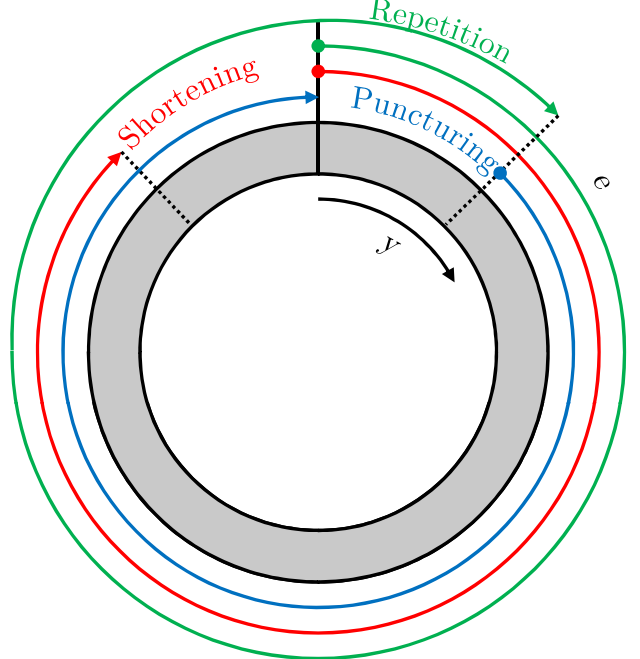


Fig. 6: Circular buffer design for rate-matching.

#### E. Encoding

The encoding is performed by the multiplication in  $\mathbb{F}_2$

$$\mathbf{d} = \mathbf{u} \cdot \mathbf{G}_N, \quad (11)$$

where  $\mathbf{G}_N = \mathbf{G}_2^{\otimes n}$ , with  $\mathbf{G}_2 = \begin{bmatrix} 1 & 0 \\ 1 & 1 \end{bmatrix}$ . Encoding complexity can be proved to be  $O(N \log N)$  [1]. However, the recursive structure of the transformation matrix suggests the possibility to have parallel implementation. If  $N/2$  processing units are available, encoding latency can be reduced to  $O(\log N)$ . A tradeoff between hardware complexity and encoding latency can be found in between.

#### F. Sub-block interleaver

The  $N$  encoded bits are then interleaved before performing the rate matching. This interleaver divides the  $N$  encoded bits stored in  $\mathbf{d}$  into 32 blocks of length  $B = \frac{N}{32}$  bits, interleaving the blocks according to a list of 32 integers  $P$  and obtaining the vector  $\mathbf{y}$  as illustrated in Figure 5. In practice, an interleaved bit  $y_j = d_i$  is calculated as  $i = B \cdot P(\lfloor j/B \rfloor) + q$ , where  $q = j \bmod B$ , for all  $j = 0, \dots, N - 1$ .

#### G. Rate matching

Rate matching is performed by a circular buffer, and the codeword  $\mathbf{e}$  of length  $E$  bits is calculated. As already men-

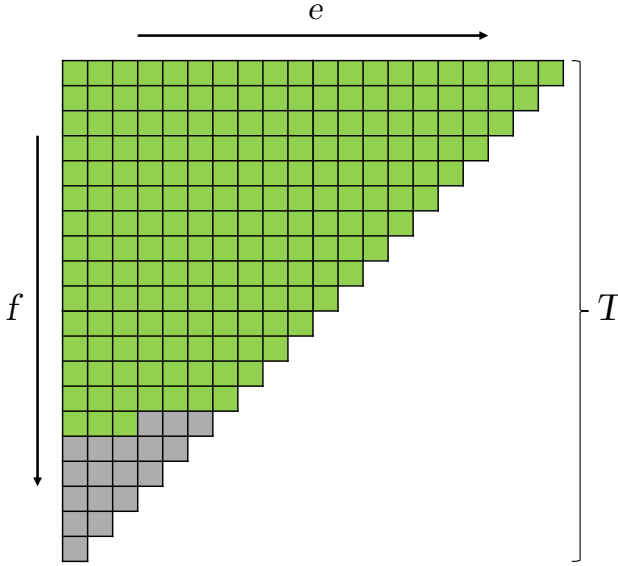


Fig. 7: Channel interleaver design.

tioned in Section III-A, three possible rate-matching schemes are foreseen:

- Puncturing: if  $E \leq N$  and  $R \leq \frac{7}{16}$ , the mother code is punctured. In this case, the first  $U = N - E$  bits are not transmitted, hence  $e_i = y_{i+U}$  for  $i = 0, \dots, E$ .
- Shortening: if  $E \leq N$  and  $R > \frac{7}{16}$ , the mother code is shortened. In this case, the last  $U = N - E$  bits are not transmitted, hence  $e_i = y_i$  for  $i = 0, \dots, E$ .
- Repetition: if  $E > N$ , the first  $U = N - E$  bits are transmitted twice, hence  $e_i = y_{i \bmod N}$  for  $i = 0, \dots, E$ .

The operating principle of the rate-matcher based on the circular buffer is illustrated in Figure 6.

#### H. Channel interleaver

Before passing the rate-matched codeword to the modulator, the bits in  $\mathbf{e}$  are interleaved one more time using a triangular bit interleaver. This interleaver has been considered necessary to improve the coding performance of the coding scheme for high-order modulation. This interleaver is not applied for every use case, and it is triggered by the parameter  $I_{BIL}$ . In particular, the channel interleaver is activated for PUCCH and PUSCH UCIs ( $I_{BIL} = 1$ ), while it is bypassed in the case of PBCH payloads and PDCCH DCIs ( $I_{BIL} = 0$ ).

The channel interleaver is formed by an isosceles triangular structure of length  $T$  bits, where  $T$  is the smallest integer such that  $\frac{T(T+1)}{2} \geq E$ ; its value can be calculated as  $T = \lceil \frac{\sqrt{8E+1}-1}{2} \rceil$ . The encoded bits in  $\mathbf{e}$  are written into the rows of the triangular structure, while the interleaved vector  $\mathbf{f}$  is obtained by reading bits out of the structure in columns. The construction of the interleaving pattern is illustrated in Figure 7. In more detail, an auxiliary  $T \times T$  matrix  $\mathbf{V}$  is created on the basis of  $\mathbf{e}$  with

$$V_{i,j} = \begin{cases} \text{NULL} & \text{if } i + j \geq T \text{ or } r(i) + j \geq E \\ e_{r(i)+j} & \text{otherwise} \end{cases} \quad (12)$$

where  $r(i) = \frac{i(2T-i+1)}{2}$ . The interleaved vector  $\mathbf{f}$  is created by appending the columns of  $\mathbf{V}$  while skipping the NULL entries. This triangular interleaver has been proposed in 5G standardization because of the practical advantages provided by its high parallelism factor, due to its maximum contention-free property, and its high flexibility.

#### IV. CONCLUSION

In this work, we have detailed the polar code encoding process within the 5<sup>th</sup> generation wireless systems standard, providing the reader with a user-friendly recipe to simulate and implement 5G-compliant polar code encoding. Upcoming extensions of this work will include decoding considerations.

#### REFERENCES

- [1] E. Arikan, "Channel polarization: A method for constructing capacity-achieving codes for symmetric binary-input memoryless channels," *IEEE Transactions on Information Theory*, vol. 55, no. 7, pp. 3051–3073, July 2009.
- [2] K. Niu, K. Chen, J. Lin, and Q. T. Zhang, "Polar codes: Primary concepts and practical decoding algorithms," *IEEE Communications magazine*, vol. 52, no. 7, pp. 192–203, July 2014.
- [3] H. Vangala, E. Viterbo, and Y. Hong, "A comparative study of polar code constructions for the awgn channel," in *arXiv preprint arXiv:1501.02473*, 2015.
- [4] R. Mori and T. Tanaka, "Performance of polar codes with the construction using density evolution," *IEEE Communications Letters*, vol. 13, no. 7, pp. 519–521, July 2009.
- [5] I. Tal and A. Vardy, "How to construct polar codes," *IEEE Transactions on Information Theory*, vol. 59, no. 10, pp. 6562–6582, October 2013.
- [6] P. Trifonov, "Efficient design and decoding of polar codes," *IEEE Transactions on Communications*, vol. 60, no. 11, pp. 3221–3227, November 2012.
- [7] M. Mondelli, S. H. Hassani, and R. Urbanke, "Construction of polar codes with sublinear complexity," in *IEEE International Symposium on Information Theory (ISIT)*, Aachen, Germany, June 2017.
- [8] G. He, J. C. Belfiore, I. Land, G. Yang, X. Liu, Y. Chen, R. Li, J. Wang, Y. Ge, R. Zhang, and W. Tong, "Beta-expansion: A theoretical framework for fast and recursive construction of polar codes," in *IEEE Global Communications Conference (GLOBECOM)*, Singapore, December 2017.
- [9] C. Condo, S. A. Hashemi, and W. J. Gross, "Efficient bit-channel reliability computation for multi-mode polar code encoders and decoders," in *2017 IEEE International Workshop on Signal Processing Systems (SiPS)*, Oct 2017, pp. 1–6.
- [10] M. Mondelli, S.H. Hassani, and R.L. Urbanke, "From polar to Reed-Muller codes: A technique to improve the finite-length performance," *IEEE Transactions on Communications*, vol. 62, no. 9, pp. 3084–3091, September 2014.
- [11] V. Bioglio, F. Gabry, I. Land, and J.-C. Belfiore, "Minimum-distance based construction of multi-kernel polar codes," in *IEEE Global Communications Conference (GLOBECOM)*, Singapore, December 2017.
- [12] M. Mondelli, S. H. Hassani, and R. L. Urbanke, "Scaling exponent of list decoders with applications to polar codes," *IEEE Transactions on Information Theory*, vol. 61, no. 9, pp. 4838–4851, September 2015.
- [13] C. Leroux, A.J. Raymond, G. Sarkis, and W.J. Gross, "A semi-parallel successive-cancellation decoder for polar codes," *IEEE Transactions on Signal Processing*, vol. 61, no. 2, pp. 289–299, January 2013.
- [14] B. L. Gal, C. Leroux, and C. Jego, "Software polar decoder on an embedded processor," in *IEEE Workshop on Signal Processing Systems (SiPS)*, Belfast, UK, October 2014.
- [15] O. Afisisadis, A. Balatsoukas-Stimming, and A. Burg, "A low-complexity improved successive cancellation decoder for polar codes," in *Asilomar Conference on Signals, Systems and Computers*, November 2014.
- [16] C. Condo, F. Ercan, and W. J. Gross, "Improved successive cancellation flip decoding of polar codes based on error distribution," in *IEEE Wireless Communications and Networking Conference (WCNC)*, Barcelona, Spain, April 2018.
- [17] I. Tal and A. Vardy, "List decoding of polar codes," *IEEE Transactions on Information Theory*, vol. 61, no. 5, pp. 2213–2226, May 2015.

[18] S. A. Hashemi, A. Balatsoukas-Stimming, P. Giard, C. Thibeault, and W. J. Gross, "Partitioned successive-cancellation list decoding of polar codes," in *IEEE International Conference on Acoustics, Speech and Signal Processing (ICASSP)*, Shanghai, China, March 2016.

[19] S. A. Hashemi, M. Mondelli, S. H. Hassani, R. L. Urbanke, and W. J. Gross, "Partitioned list decoding of polar codes: Analysis and improvement of finite length performance," in *IEEE Global Communications Conference (GLOBECOM)*, Singapore, December 2017.

[20] S. A. Hashemi, C. Condo, F. Ercan, and W. J. Gross, "Memory-efficient polar decoders," *IEEE Journal on Emerging and Selected Topics in Circuits and Systems*, vol. 70, no. 4, pp. 604–615, April 2017.

[21] K. Niu and K. Chen, "Stack decoding of polar codes," *Electronics Letters*, vol. 48, no. 12, pp. 695–697, June 2012.

[22] B. Li, H. Shen, and D. Tse, "An adaptive successive cancellation list decoder for polar codes with cyclic redundancy check," *IEEE Communications Letters*, vol. 16, no. 12, pp. 2044–2047, December 2012.

[23] C. Condo, S. A. Hashemi, A. Ardakani, F. Ercan, and W. J. Gross, "Design and implementation of a polar codes blind detection scheme," in *arXiv preprint arXiv:1801.01820*, January 2018.

[24] G. Sarkis, P. Giard, A. Vardy, C. Thibeault, and W. J. Gross, "Fast polar decoders: Algorithm and implementation," *IEEE Journal on Selected Areas in Communications*, vol. 32, no. 5, pp. 946–957, May 2014.

[25] M. Hanif and M. Ardakani, "Fast successive-cancellation decoding of polar codes: Identification and decoding of new nodes," *IEEE Communication Letters*, vol. 21, no. 11, pp. 2360–2363, November 2017.

[26] P. Giard and A. Burg, "Fast-SSC-flip decoding of polar codes," in *arXiv preprint arXiv:1712.00256*, 2017.

[27] S. A. Hashemi, C. Condo, and W. J. Gross, "Simplified successive-cancellation list decoding of polar codes," in *IEEE International Symposium on Information Theory (ISIT)*, Barcelona, Spain, July 2016.

[28] S. A. Hashemi, C. Condo, and W. J. Gross, "A fast polar code list decoder architecture based on sphere decoding," *IEEE Transactions on Circuits and Systems I: Regular Papers*, vol. 63, no. 12, pp. 2368–2380, December 2016.

[29] S. A. Hashemi, C. Condo, and W. J. Gross, "Fast simplified successive-cancellation list decoding of polar codes," in *IEEE Wireless Communications and Networking Conference (WCNC)*, San Francisco, CA, USA, March 2017.

[30] S. A. Hashemi, C. Condo, and W. J. Gross, "Fast and flexible successive-cancellation list decoders for polar codes," *IEEE Transactions on Signal Processing*, vol. 65, no. 21, pp. 5756–5769, October 2017.

[31] K. K. Yuan, B. and. Parhi, "Low-latency successive-cancellation polar decoder architectures using 2-bit decoding," *IEEE Transactions on Circuits and Systems I: Regular Papers*, vol. 61, no. 4, pp. 1241–1254, April 2014.

[32] C. Xiong, J. Lin, and Z. Yan, "Symbol-based successive cancellation list decoder for polar codes," in *IEEE Workshop on Signal Processing Systems (SiPS)*, Belfast, UK, October 2014.

[33] N. Goela, S. B. Korada, and M. Gastpar, "On LP decoding of polar codes," in *IEEE Information Theory Workshop (ITW)*, Dublin, Ireland, August 2010.

[34] V. Tarantalli and P. H. Siegel, "Adaptive linear programming decoding of polar codes," in *IEEE International Symposium on Information Theory (ISIT)*, Hawaii, U.S.A., July 2014.

[35] S. Cammerer, M. Ebada, A. Elkelesh, and S. T. Brink, "Sparse graphs for belief propagation decoding of polar codes," in *arXiv preprint arXiv:1712.08538*, 2017.

[36] T. Richardson and R. Urbanke, *Modern Coding Theory*, Cambridge University Press, 2008.

[37] V. Bioglio, F. Gabry, and I. Land, "Low-complexity puncturing and shortening of polar codes," in *IEEE Wireless Communications and Networking Conference (WCNC)*, San Francisco, USA, March 2017.

[38] D. M. Shin, S. C. Lim, and K. Yang, "Design of length-compatible polar codes based on the reduction of polarizing matrices," *IEEE Transactions on Communications*, vol. 61, no. 7, pp. 2593–2599, July 2013.

[39] R. Wang and R. Liu, "A novel puncturing scheme for polar codes," *IEEE Communications Letters*, vol. 18, no. 12, pp. 2081–2084, December 2014.

[40] L. Chandresris, V. Savin, and D. Declercq, "On puncturing strategies for polar codes," in *IEEE International Conference on Communications (ICC)*, Paris, France, May 2017.

[41] L. Zhang, Z. Zhang, X. Wang, Q. Yu, and Y. Chen, "On the puncturing patterns for punctured polar codes," in *IEEE International Symposium on Information Theory (ISIT)*, Hawaii, U.S.A., July 2014.

[42] H. Saber and I. Marsland, "An incremental redundancy hybrid ARQ scheme via puncturing and extending of polar codes," *IEEE Transactions on Communications*, vol. 63, no. 11, pp. 3964–3973, November 2015.

[43] V. Miloslavskaya, "Shortened polar codes," *IEEE Transactions on Information Theory*, vol. 61, no. 9, pp. 4852–4865, September 2015.

[44] K. Niu and K. Chen, "CRC-aided decoding of polar codes," *IEEE Communications Letters*, vol. 16, no. 10, pp. 1668–1671, October 2012.

[45] T. Wang, D. Qu, and T. Jiang, "Parity-check-concatenated polar codes," *IEEE Communications Letters*, vol. 20, no. 12, pp. 2342–2345, December 2016.

[46] P. Yuan, T. Prinz, and G. Bocherer, "Polar code construction for list decoding," in *arXiv preprint arXiv:1707.09753*, 2017.

[47] Peter Trifonov and Vera Miloslavskaya, "Polar codes with dynamic frozen symbols and their decoding by directed search," *CoRR*, vol. abs/1307.2352, 2013.

[48] J. Park and H. Y. Kim, I. and Song, "Construction of parity-check-concatenated polar codes based on minimum hamming weight codewords," *Electronics Letters*, vol. 53, no. 14, pp. 924–926, July 2017.

[49] H. Zhang, R. Li, J. Wang, S. Dai, G. Zhang, Y. Chen, H. Luo, and J. Wang, "Parity-check polar coding for 5G and beyond," in *arXiv preprint arXiv:1801.03616*, January 2018.

[50] M. Xu, P. Chen, B. Bai, and S. Tong, "Distance spectrum and optimized design of concatenated polar codes," in *International Conference on Wireless Communications and Signal Processing (WCSP)*, Nanjing, China, October 2017.

[51] G. Ricciutelli, M. Baldi, F. Chiaraluce, and G. Liva, "On the error probability of short concatenated polar and cyclic codes with interleaving," in *IEEE International Symposium on Information Theory (ISIT)*, Aachen, Germany, June 2017.

[52] J. Chen, Y. Chen, K. Jayasinghe, D. Du, and J. Tan, "Distributing CRC bits to aid polar decoding," in *IEEE Global Communications Conference (GLOBECOM)*, Singapore, December 2017.

[53] M. Seidl, A. Schenk, C. Stierstorfer, and J. B. Huber, "Polar-coded modulation," *IEEE Transactions on Communications*, vol. 61, no. 10, pp. 4108–4119, October 2013.

[54] G. Bocherer, T. Prinz, P. Yuan, and F. Steiner, "Efficient polar code construction for higher-order modulation," in *IEEE Wireless Communications and Networking Conference (WCNC)*, San Francisco, USA, March 2017.

[55] P. Chen, M. Xu, B. Bai, and X. Ma, "Design of polar coded 64-QAM," in *IEEE International Symposium on Turbo Codes and Iterative Information Processing (ISTC)*, Brest, France, September 2016.

[56] H. Mahdavifar, M. El-Khamy, J. Lee, and I. Kang, "Polar coding for bit-interleaved coded modulation," *IEEE Transactions on Vehicular Technology*, vol. 65, no. 5, pp. 3115–3127, May 2016.

[57] H. Afser, N. Tirpan, H. Delic, and M. Koca, "Bit-interleaved polar-coded modulation," in *IEEE Wireless Communications and Networking Conference (WCNC)*, Istanbul, Turkey, April 2014.

[58] K. Chen, K. Niu, and J. R. Lin, "An efficient design of bit-interleaved polar coded modulation," in *IEEE Personal Indoor and Mobile Radio Communications (PIMRC)*, London, UK, September 2013.

[59] D. M. Shin, S. C. Lim, and K. Yang, "Mapping selection and code construction for 2<sup>m</sup>-ary polar-coded modulation," *IEEE Communications Letters*, vol. 16, no. 6, pp. 905–908, June 2012.

[60] T. Koike-Akino, Y. Wang, S. C. Draper, K. Sugihara, and W. Matsumoto, "Bit-interleaved polar-coded OFDM for low-latency M2M wireless communications," in *IEEE International Conference on Communications (ICC)*, Paris, France, May 2017.

[61] K. Tian, R. Liu, and R. Wang, "Joint successive cancellation decoding for bit-interleaved polar coded modulation," *IEEE Communications Letters*, vol. 20, no. 2, pp. 224–227, February 2016.

[62] 3<sup>rd</sup> Generation Partnership Project (3GPP), "Technical specification group radio access network," *3GPP TS 38.212 V15.0.0*, 2017.

[63] 3<sup>rd</sup> Generation Partnership Project (3GPP), "Multiplexing and channel coding," *3GPP 38.212 V15.1.0*, 2018.

[64] 3GPP TSG RAN WG1 #90, "Summary of email discussion [NRAH2-11] polar code sequence," [http://www.3gpp.org/ftp/tsg\\_ran/wg1\\_r11/TSGR1\\_90/Docs/R1-1712174.zip](http://www.3gpp.org/ftp/tsg_ran/wg1_r11/TSGR1_90/Docs/R1-1712174.zip), Prague, Czech Republic, August 2017.

[65] A. Eslami and H. Pishro-Nik, "On finite-length performance of polar codes: stopping sets, error floor, and concatenated design," *IEEE Transactions on Communications*, vol. 61, no. 3, pp. 919–929, March 2013.